CONFIDENTIAL

Copy
RM L54E03a

NACA

RESEARCH MEMORANDUM

STRESSES AND DEFLECTIONS OF A SWEPT BIPLANE WING

By George W. Zender and John E. Duberg

Langley Aeronautical Laboratory
Langley Field, Va.

NATIONAL ADVISORY COMMITTEE
FOR AERONAUTICS

WASHINGTON
August 3, 1954

CONFIDENTIAL

NATIONAL ADVISORY COMMITTEE FOR AERONAUTICS

RESEARCH MEMORANDUM

STRESSES AND DEFLECTIONS OF A SWEPT BIPLANE WING

By George W. Zender and John E. Duberg

SUMMARY

The results of experimental and theoretical structural studies of a solid swept biplane wing composed of a sweptback front wing and a sweptforward rear wing joined at the tip are compared. The 45° swept biplane with wings of 4-percent thickness is structurally comparable to the solid 45° swept monoplane wing of between 2- and 4-percent thickness.

INTRODUCTION

One of the configurations which has recently been of some interest is the swept biplane wing. Among the types of swept biplane wing under consideration is that which consists of a sweptback front wing with the root attached near the upper forward part of the fuselage and with the tip joined to the tip of a sweptforward rear wing with root attached near the lower rear part of the fuselage. Wind-tunnel tests (ref. 1) of models of this type at subsonic and transonic speeds have shown some favorable aerodynamic characteristics as compared with swept wings, particularly with regard to pitch-up tendencies.

In order to obtain information on the structural behavior of the swept biplane wing, stress and deflection measurements of a model of this wing were obtained for bending and twisting loads. The purpose of this paper is to compare the results of these tests with a theoretical method for the calculation of the stresses and deflections. In addition, some structural comparisons of the swept biplane configuration with swept monoplane configurations are presented.

SYMBOLS

α	angle of attack due to loads
θ	angle of twist (see fig. 11)

Λ	angle of sweep, deg
γ	dihedral angle (see fig. 2), deg
ψ	slope at root triangle (see appendix)
λ	Lagrangian multiplier
ϕ	constraining or equilibrium function (see appendix)
c	root chord (see appendix), in.
h	semi-gap at rigid tip (see fig. 2)
A	area, $in.^2$
E	modulus of elasticity, psi
G	modulus of rigidity, psi
I	moment of inertia, $in.^4$
J	torsion constant, $in.^4$
l	semispan of wing (see fig. 2), in.
L	length of beam (see fig. 9), in.
M	bending moment, in-lb
T	torque, in-lb
p	local wing loading, lb/in.
P	force, lb
x	distance along beam from origin (see fig. 9), in.
ξ	distance from root (see fig. 2), in.
w	upward deflection, in.
$w_{n_{F,R}(\xi)}$	deflection at gage location n caused by application of a unit load on center line of front (or rear) wing at station ξ, in./lb
σ	normal stress, psi or ksi
$\sigma_{n_{F,R}(\xi)}$	stress at gage location n caused by application of a unit load on center line of front (or rear) wing at station ξ, psi/lb

Subscripts:

n	specific gage locations shown in figures
x,y,z	coordinate axes
AL	applied load
F	front
R	rear
V,H,W,T	type of stress component (see fig. 6)

TEST SPECIMEN AND METHOD OF TESTING

The swept-biplane-wing model shown in figure 1 was formed from a single piece of steel plate to the dimensions shown in figure 2. The root of each wing (front and rear) of the model was clamped between the support blocks shown in figure 1. A concentrated lift load was applied at the center line of the cross section at each of five spanwise locations on the front and rear wings. Longitudinal strains were obtained at the locations shown in figure 3 with Baldwin SR-4 type A-7 strain gages and the deflections were obtained with dial indicators of 0.0001-inch least division at the locations shown in figure 4. In addition, a pure torque was applied near the tip of the front wing of the swept biplane wing as shown in figure 5. The longitudinal strains were obtained in the same manner as for the lift loads at the locations shown in figure 3 and deflections were obtained at the locations shown in figure 5.

The longitudinal strains for both the lift and torque loads were converted to stress by multiplying by $E = 30 \times 10^6$ psi; the effect of the transverse stresses on this conversion were neglected, the gages being located near the edge of the plate.

EXPERIMENTAL RESULTS

The experimental deflections and stresses for the lift loads are given in tables I and II, respectively, in the form of deflection and stress influence coefficients, that is, the deflection and stress at the various gage locations due to unit loads on the center line at the indicated stations, ξ. In order to approximate a more realistic loading of the swept biplane wing, the data given in tables I and II were used to obtain data for an elliptically distributed loading along the 17-inch

semispan. Two-thirds of the elliptically distributed loading was assumed to be supported by the front wing and the remaining one-third by the rear wing. The loading at the root of the front wing was assumed to be $\cos \Lambda$ and at the root of the rear wing $1/2 \cos \Lambda$. The front-wing loading then is given by $p_F = \cos \Lambda \sqrt{1 - \left(\frac{\xi}{l}\right)^2}$ and the rear-wing loading by $p_R = \frac{1}{2} \cos \Lambda \sqrt{1 - \left(\frac{\xi}{l}\right)^2}$. The total lift load on the biplane semispan is then 20.03 pounds.

The deflections w_n, at the various gage locations n, due to the elliptically distributed loading were obtained by the following formula:

$$w_n = w_{n_F} + w_{n_R}$$

in which

$$w_{n_{F,R}} = \frac{1}{\cos \Lambda} \int_0^l p_{F,R} w_{n_{F,R}}(\xi) d\xi$$

where $w_{n_F}(\xi)$ and $w_{n_R}(\xi)$ are the influence coefficients for loads on the front and rear wings, respectively, given in table I. The quantity w_{n_F} represents the deflection at the particular gage location due to the load on the front wing while the quantity w_{n_R} represents the deflection at the same gage location due to the load on the rear wing. The integrals for w_{n_F} and w_{n_R} were evaluated mechanically and the results are given in table III. The same procedure when applied to the stresses produced the values of σ_n shown in table IV. The deflections and stresses for the pure torque load were reduced for unit torque load and are presented in tables V and VI, respectively.

A more significant stress picture is obtained if the stresses shown in tables IV and VI are separated into four components associated with stress distributions of the type shown in figure 6. One stress component is associated with normal bending identified by the symbol σ_V while another bending action, particularly significant in the swept biplane wing when compared with more conventional configurations, is the chordwise type of

bending designated σ_H in figure 6. Another stress component is associated with direct extension or contraction represented by the symbol σ_T in figure 6 while the fourth stress component σ_W is due to restraint of warping of the cross section (these stresses are often called bending stresses due to torsion). By using the four stresses on each cross section normal to the leading or trailing edge given in tables IV and VI, it is possible to solve for the magnitude of the four stress components. The values obtained for the stress components are given by the test points in figures 7 and 8.

THEORETICAL ANALYSIS

An analysis, given in the appendix, of the swept-biplane configuration was made by means of a strain-energy approach. The analysis was applied to the particular cases of the elliptically distributed lift loading of 20.03 pounds and the unit torque loading. The structure considered was broken up as shown in figure 9. The tip part was assumed to be rigid, the triangular-root parts were considered in the same manner as given in reference 2, and the parts of the elliptically distributed loading acting in the triangular-root parts were neglected. The intermediate front and rear beams were assumed to behave according to elementary beam theory. The unknowns in the analysis are the forces and moments on the cut sections shown in figure 9. The values of these quantities are given in table VII for the 20.03-pound elliptically distributed loading and in table VIII for the unit torque load. With these forces and moments known, the stresses and deflections can be computed.

COMPARISON OF THEORY AND EXPERIMENT

Stresses

Bending.- The experimental and theoretical stress components for the elliptically distributed lift load of 20.03 pounds are compared in figure 7. The theoretical stresses shown by the solid curves in figure 7 are obtained from the elementary formulas M_y/I or P/A evaluated for the entire loading, that is, the three components of the applied elliptically distributed loading and the forces and moments at the cut sections. The warping stresses σ_W are not given by the theory but an approximation may be made by introducing the twisting moments at the cut sections into the equation at the bottom of page 13 of reference 3. The σ_W stresses obtained by this approximation are given by the solid line on the plots for σ_W in figure 7. The bending stresses σ_V and σ_H for both the front

and rear wings comprise the main portion of the total stresses. The σ_T stresses are negligible as compared with the other three components. The effect of having the front and rear wings joined at the tip is indicated by a comparison of the biplane stresses with the unjoined tip or cantilever stresses given by the dashed lines in figure 7. Joining the tips causes an appreciable reduction in the σ_V stresses of both the front and rear wings with a small increase in the σ_H stresses.

Torsion.- The experimental and theoretical stress components for the unit torque load are compared in figure 8. The theoretical stresses are obtained from the elementary formulas M_y/I or P/A for the forces and moments at the cut sections. The warping stresses σ_W were approximated in the same manner as for the bending loads.

DEFLECTIONS, ANGLES OF ATTACK, AND TWISTS

Bending.- The solid curves in figure 10 show the theoretical center-line deflections for the elliptically distributed lift load of 20.03 pounds. These deflections were obtained by superposing the deflections of the beam parts of the wings on the deflections due to the flexibility of the root triangle. Elementary beam theory was used for the beam parts and the root triangle was treated by the method of reference 2. In these calculations only the component of the applied loading normal to the wing surface and the P_z forces and M_y moments at the cut sections were included. The effect on the vertical deflections of the other components of the loading and the transverse and longitudinal shears and moments at the cut sections was negligible. The theoretical center-line deflections in figure 10 are seen to underestimate the experimental deflections. The difference appears to be largely due to the approximation of the contribution of the triangular-root parts to the deflections of the outer parts. The approximation for the effects of the triangular-root distortions on the deflections of the outer part of the wing were of sufficient accuracy for the cantilever types of wing configurations of reference 2 since they represented a small part of the total deflections of the outer part. The deflections, however, of the beam parts of the biplane wing due to the applied loads are largely canceled by the deflections due to the P_z forces and M_y moments at the cut sections with the result that the deflections due to the triangular-root parts represent a large part of the total deflections (in this case approx. 60 percent of the total tip deflection).

The theoretical angles of attack shown by the solid curves in figure 10 were evaluated from the elementary beam equations in the same manner as the deflections and are compared with the experimental angles of attack.

The effect of having the front and rear wings joined at the tip is again indicated by a comparison of the biplane deflections and angles of attack with the cantilever values given by the dashed lines in figure 10. The cantilever deflections and angles of attack are the distortions that would occur if the front and rear wings were not joined at the tip. However, when the tips are joined, the cantilever distorsions are opposed by the distortions due to the tip loads; the result is smaller total distortions for the biplane configuration.

Torsion.- The structural twists θ are obtained from the elementary equation Tx/GJ for the applied torque T and the M_X values at the cut sections. In addition, the twist of the front and rear beams contributed by the triangular-root parts is included by the method of reference 2. The experimental and theoretical twists θ are compared in figure 11. The deflections of the center line due to the torque load are very small and therefore are not presented.

Again, the effect of joining the front and rear wings at the tip is indicated by the cantilever (dashed curves) and biplane (solid curves) values of the structural twist θ. The effect of the M_X load is to reduce appreciably the twists of the front wing and in addition to produce a slight twist of the rear wing.

COMPARISON OF SWEPT BIPLANE WING WITH SWEPT MONOPLANE WING

In order to relate the swept biplane wing structurally with the swept monoplane configuration, the information obtained for the particular biplane configuration discussed herein was compared with swept monoplane configurations of the proportions shown in figure 12. The proportions of the swept biplane wing are also shown in figure 12 for comparison purposes. The models have equal spans and lifting areas and consequently equal aspect ratios. The 4-percent-thick swept biplane wing is derived from the 2-percent-thick swept monoplane wing by placing the rear half of the monoplane wing into the position shown for the rear wing of the biplane, while the 4-percent-thick swept monoplane configuration is comparable in frontal area to the swept biplane configuration. In addition, the 6-percent-thick swept monoplane configuration is included since reference 1 includes aerodynamic comparisons for a 6-percent-thick swept monoplane with a 4-percent-thick swept biplane configuration.

The deflections and angles of attack for the swept monoplane configurations for an elliptically distributed lift loading of 20.03 pounds computed by the method of reference 2 are shown by the dashed lines in figure 13. The agreement of experiment and theory presented in reference 2

permits confidence in the accuracy of the computed values for the swept monoplane models. The deflections and angles of attack of the biplane configuration (experimental) are shown by the test points in figure 13. The deflections of the 4-percent-thick swept biplane fit between the deflection curves for the 2-percent-thick and 4-percent-thick swept monoplane models. The angles of attack of the front and rear biplane wings are of opposite sign over most of the span and reach their largest absolute values at about one-fourth the semispan. The absolute values of the angle of attack of the swept biplane over most of the span are bracketed by the angles of attack of the 2-percent- and 4-percent-thick models. Based on solid sections then, the deflections and angles of attack due to wing loads of the swept biplane configuration are comparable to the swept monoplane wing of between 2-percent and 4-percent thickness.

A structural comparison of the swept biplane and monoplane configurations on the basis of stresses is more involved than the comparison made on the basis of deflections and angles of attack. In addition, the secondary stress effects are much more important in the case of box-type structures than for solid structures so that stress comparisons based on solid sections might not be especially significant. However, some information is available in a comparison of the primary stresses of the swept biplane and monoplane wings of figure 12. The bending stress component σ_y for the 4-percent-thick swept biplane is shown by the test points in figure 14 for the elliptically distributed lift load of 20.03 pounds. The M_y/I stresses for the same lift load on the swept monoplane wings of figure 12 are shown by the dashed lines of figure 14. It is apparent that, near the root, the σ_y values for the 4-percent-thick swept biplane wing are between the stresses for the 2-percent- and 4-percent-thick swept monoplane wings.

CONCLUDING REMARKS

A method has been described for the stress and distortion analysis of a swept biplane wing and the results of the method are compared with experiment. Satisfactory agreement of experiment and theory is obtained except for the deflections where the differences of the theory and experiment are primarily due to the inaccuracy of the assumptions made regarding the triangular-root parts of the front and rear wings. While these assumptions have a minor effect on the stresses of the biplane wing, their effect on the deflections is appreciable.

An investigation of the solid 45° swept biplane of 4-percent thickness indicates that the configuration is structurally comparable to a solid 45° swept monoplane of between 2- and 4-percent thickness.

Preliminary wind-tunnel data have indicated that the drag of the 4-percent-thick swept biplane wing—body configuration is approximately the same as the 6-percent-thick swept monoplane wing—body configuration at transonic speeds; since the 6-percent-thick swept monoplane configuration evidently has a stiffer wing, there is doubt as to the usefulness of the swept-biplane-wing configuration. However, it should be noted that the objectionable pitch-up tendencies of the swept-monoplane-wing configuration are not experienced by the swept-biplane-wing configuration; the advantage of this elimination of the pitch-up tendency may well outweigh the stress and distortion advantages of the swept monoplane. In addition, other considerations might favor the swept-biplane-wing configuration such as weight saving of tail surfaces and favorable wing-body designs resulting from applications of the transonic area rule.

Langley Aeronautical Laboratory,
National Advisory Committee for Aeronautics,
Langley Field, Va., April 22, 1954.

APPENDIX

An analysis of the swept biplane wing based on the minimum complementary energy principle may be developed by considering the five component parts of the biplane shown in figure 9. The five parts are the front and rear beams, the front and rear root triangles, and the tip part which is assumed rigid. The unknowns in the analysis are the forces and moments shown on the cut sections at the rigid tip in figure 9. Since the cut sections are inclined slightly due to the geometry of the wing configuration, the forces and moments on the cut sections are inclined to the vertical and horizontal as indicated in figure 9. In addition, since the applied loads on the structure are in the vertical plane, the components of the loads in the planes of the inclined axes are used in the analysis.

The front and rear beam parts of the biplane wing are assumed to be loaded as shown in figure 9 and the strain energy due to these loads is given by

$$S.E. = \int_0^L \left[M_{AL_y} + M_y + P_z(L - x)\right]^2 \frac{dx}{2EI_y} + \int_0^L \left[M_{AL_z} + M_z + P_y(L - x)\right]^2 \frac{dx}{2EI_z} + \int_0^L \left[\mp P_{AL_x} + P_x\right]^2 \frac{dx}{2EA} + \int_0^L \left[M_{AL_x} + M_x\right]^2 \frac{dx}{2GJ} \tag{1}$$

(Negative sign is required in the third integral for the front beam since the component of applied load is in the opposite direction to the axial force P_x; conversely, a positive sign is required for the rear beam.)

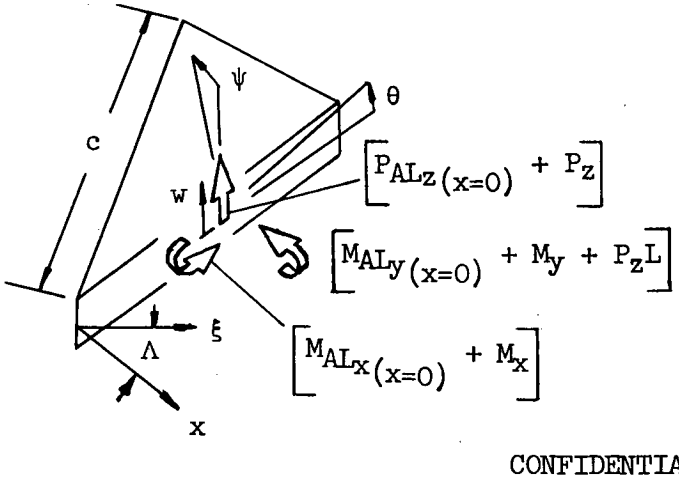

The loads assumed on the root triangle (the effect of loads not shown is assumed negligible) are as shown on the sketch to the left. The strain energy of the root triangle due to these loads is then given by

$$S.E. = \left[P_{AL_z(x=0)} + P_z\right]\frac{w_P}{2} + \left[M_{AL_y(x=0)} + M_y + P_zL\right]\frac{\psi_M}{2} + \left[P_{AL_z(x=0)} + P_z\right]w_M +$$

$$\left[M_{AL_x(x=0)} + M_x\right]\frac{\theta_T}{2} + \left[P_{AL_z(x=0)} + P_z\right]w_T + \left[M_{AL_y(x=0)} + M_y + P_zL\right]\psi_T \qquad (2)$$

From equations (A16), (A17), (A20), and (A21) of reference 2,

$$\left.\begin{aligned}
w_P &= \frac{c^3\sin^3\Lambda\cos^4\Lambda}{16EI_y}\left[P_{AL_z(x=0)} + P_z\right] \\
w_M &= \frac{c^2\sin^3\Lambda\cos^3\Lambda}{6EI_y\tan\Lambda}\left[M_{AL_y(x=0)} + M_y + P_zL\right] \\
w_T &= \frac{c^2\sin^3\Lambda\cos^3\Lambda}{6EI_y}\left[M_{AL_x(x=0)} + M_x\right] \\
\theta_T &= \frac{c\sin^3\Lambda\cos^2\Lambda}{2EI_y}\left[M_{AL_x(x=0)} + M_x\right] \\
\psi_M &= \frac{c\sin^2\Lambda\cos^3\Lambda}{2EI_y\tan\Lambda}\left[M_{AL_y(x=0)} + M_y + P_zL\right] \\
\psi_T &= \frac{c\sin^2\Lambda\cos^3\Lambda}{2EI_y}\left[M_{AL_x(x=0)} + M_x\right]
\end{aligned}\right\} \qquad (3)$$

Substitution of equations (3) into equation (2) gives for the root triangle

$$\text{S.E.} = \left[P_{AL_z(x=0)} + P_z\right]^2 \frac{c^3 \sin^3\Lambda \cos^4\Lambda}{32EI_y} + \left[M_{AL_y(x=0)} + M_y + P_z L\right]^2 \frac{c \sin^2\Lambda \cos^3\Lambda}{4EI_y \tan\Lambda} + \left[P_{AL_z(x=0)} + P_z\right]\left[M_{AL(x=0)} + M_y + P_z L\right] \frac{c^2 \sin^3\Lambda \cos^3\Lambda}{6EI_y \tan\Lambda} + \left[M_{AL_x(x=0)} + M_x\right]^2 \frac{c \sin^3\Lambda \cos^2\Lambda}{4EI_y} + \left[P_{z(x=0)} + P_z\right]\left[M_{AL_x(x=0)} + M_x\right] \frac{c^2 \sin^3\Lambda \cos^3\Lambda}{6EI_y} + \left[M_{AL_y(x=0)} + M_y + P_z L\right]\left[M_{AL_x(x=0)} + M_x\right] \frac{c \sin^2\Lambda \cos^3\Lambda}{2EI_y} \qquad (4)$$

The total strain energy of the swept biplane wing may be obtained from the sum of the strain energies of the front and rear wings (eq. (1)) and the front and rear root triangles (eq. (4)). The total strain energy is

$$\text{S.E.} = \int_0^{L_F} \left[M_{AL_{y_F}} + M_{y_F} + P_{z_F}\left(L_F - x_F\right)\right]^2 \frac{dx_F}{2EI_{y_F}} + \int_0^{L_F} \left(-P_{AL_{x_F}} + P_{x_F}\right)^2 \frac{dx_F}{2EA_F} + \int_0^{L_F} \left[M_{AL_{z_F}} + M_{z_F} + P_{y_F}\left(L_F - x_F\right)\right]^2 \frac{dx_F}{2EI_{z_F}} + \int_0^{L_F} \left(M_{AL_{x_F}} + M_{x_F}\right)^2 \frac{dx_F}{2GJ_F} + \int_0^{L_R} \left[M_{AL_{y_R}} + M_{y_R} + P_{z_R}\left(L_R - x_R\right)\right]^2 \frac{dx_R}{2EI_{y_R}} + \int_0^{L_R} \left(P_{AL_{x_R}} + P_{x_R}\right)^2 \frac{dx_R}{2EA_R} + \int_0^{L_R} \left[M_{AL_{z_R}} + M_{z_R} + P_{y_R}\left(L_R - x_R\right)\right]^2 \frac{dx_R}{2EI_{z_R}} + \int_0^{L_R} \left(M_{AL_{x_R}} + M_{x_R}\right)^2 \frac{dx_R}{2GJ_R} +$$

(equation continued on next page)

$$\left[\left[P_{AL_{z(x=0)_F}} + P_{z_F}\right]^2 \frac{c_F^3 \sin^3\Lambda_F \cos^4\Lambda_F}{32EI_{y_F}} + \left(M_{AL_{y(x=0)_F}} + M_{y_F} + P_{z_F}L_F\right)^2 \frac{c_F \sin^2\Lambda_F \cos^3\Lambda_F}{4EI_{y_F} \tan\Lambda_F} + \left[P_{AL_{z(x=0)_F}} + P_{z_F}\right]\left[M_{AL_{y(x=0)_F}} + M_{y_F} + P_{z_F}L_F\right]\frac{c_F^2 \sin^3\Lambda_F \cos^3\Lambda_F}{6EI_{y_F} \tan\Lambda_F} + \left[M_{AL_{x(x=0)_F}} + M_{x_F}\right]^2 \frac{c_F \sin^3\Lambda_F \cos^2\Lambda_F}{4EI_{y_F}} + \left[P_{AL_{z(x=0)_F}} + P_{z_F}\right]\left[M_{AL_{x(x=0)_F}} + M_{x_F}\right]\frac{c_F^2 \sin^3\Lambda_F \cos^3\Lambda_F}{6EI_{y_F}} + \left[M_{AL_{y(x=0)_F}} + M_{y_F} + P_{z_F}L_F\right]\left[M_{AL_{x(x=0)_F}} + M_{x_F}\right]\frac{c_F \sin^2\Lambda_F \cos^3\Lambda_F}{2EI_{y_F}} + \left[P_{AL_{z(x=0)_R}} + P_{z_R}\right]^2 \frac{c_R^3 \sin^3\Lambda_R \cos^4\Lambda_R}{32EI_{y_R}} + \left[M_{AL_{y(x=0)_R}} + M_{y_R} + P_{z_R}L_R\right]^2 \frac{c_R \sin^2\Lambda_R \cos^3\Lambda_R}{4EI_{y_R} \tan\Lambda_R} + \left[P_{AL_{z(x=0)_R}} + P_{z_R}\right]\left[M_{AL_{y(x=0)_R}} + M_{y_R} + P_{z_R}L_R\right]\frac{c_R^2 \sin^3\Lambda_R \cos^3\Lambda_R}{6EI_{y_R} \tan\Lambda_R} + \left[M_{AL_{x(x=0)_R}} + M_{x_R}\right]^2 \frac{c_R \sin^3\Lambda_R \cos^2\Lambda_R}{4EI_{y_R}} + \left[P_{AL_{z(x=0)_R}} + P_{z_R}\right]\left[M_{AL_{x(x=0)_R}} + M_{x_R}\right]\frac{c_R^2 \sin^3\Lambda_R \cos^3\Lambda_R}{6EI_{y_R}} + \left[M_{AL_{y(x=0)_R}} + M_{y_R} + P_{z_R}L_R\right]\left[M_{AL_{x(x=0)_R}} + M_{x_R}\right]\frac{c_R \sin^2\Lambda_R \cos^3\Lambda_R}{2EI_{y_R}}\right] \quad (5)$$

where the terms within the dashed brackets are those due to the front and rear root triangles.

There are six equations of equilibrium among the unknown forces and moments on the rigid tip shown in figure 9. These equilibrium conditions are for the transverse forces,

$$\phi_1 = \frac{\cos \Lambda_F P_{x_F} L_F}{L_F\sqrt{1 + \cos^2\Lambda_F \tan^2\gamma_F}} - \frac{\cos \gamma_F \sin \Lambda_F P_{y_F} L_F}{L_F\sqrt{1 + \cos^2\Lambda_F \tan^2\gamma_F}} + \frac{\sin \gamma_F P_{z_F} L_F}{L_F} +$$

$$\frac{\cos \Lambda_R P_{x_R} L_R}{L_R\sqrt{1 + \cos^2\Lambda_R \tan^2\gamma_R}} + \frac{\cos \gamma_R \sin \Lambda_R P_{y_R} L_R}{L_R\sqrt{1 + \cos^2\Lambda_R \tan^2\gamma_R}} - \frac{\sin \gamma_R P_{z_R} L_R}{L_R} = 0 \qquad (6)$$

for the vertical forces,

$$\phi_2 = \frac{\cos \Lambda_F \tan \gamma_F P_{x_F} L_F}{L_F\sqrt{1 + \cos^2\Lambda_F \tan^2\gamma_F}} - \frac{\sin \gamma_F \sin \Lambda_F P_{y_F} L_F}{L_F\sqrt{1 + \cos^2\Lambda_F \tan^2\gamma_F}} - \frac{\cos \gamma_F P_{z_F} L_F}{L_F} -$$

$$\frac{\cos \Lambda_R \tan \gamma_R P_{x_R} L_R}{L_R\sqrt{1 + \cos^2\Lambda_R \tan^2\gamma_R}} - \frac{\sin \gamma_R \sin \Lambda_R P_{y_R} L_R}{L_R\sqrt{1 + \cos^2\Lambda_R \tan^2\gamma_R}} - \frac{\cos \gamma_R P_{z_R} L_R}{L_R} = 0 \qquad (7)$$

for the longitudinal forces,

$$\phi_3 = \frac{\sin \Lambda_F P_{x_F} L_F}{L_F\sqrt{1 + \cos^2\Lambda_F \tan^2\gamma_F}} + \frac{\cos \Lambda_F P_{y_F} L_F}{L_F \cos \gamma_F\sqrt{1 + \cos^2\Lambda_F \tan^2\gamma_F}} -$$

$$\frac{\sin \Lambda_R P_{x_R} L_R}{L_R\sqrt{1 + \cos^2\Lambda_R \tan^2\gamma_R}} + \frac{\cos \Lambda_R P_{y_R} L_R}{L_R \cos \gamma_R\sqrt{1 + \cos^2\Lambda_R \tan^2\gamma_R}} = 0 \qquad (8)$$

for the rolling moments,

$$\phi_4 = \frac{\sin \Lambda_F M_{x_F}}{\sqrt{1 + \cos^2\Lambda_F \tan^2\gamma_F}} + \frac{\cos \Lambda_F M_{y_F}}{\cos \gamma_F \sqrt{1 + \cos^2\Lambda_F \tan^2\gamma_F}} -$$

$$\frac{\sin \Lambda_R M_{x_R}}{\sqrt{1 + \cos^2\Lambda_R \tan^2\gamma_R}} + \frac{\cos \Lambda_R M_{y_R}}{\cos \gamma_R \sqrt{1 + \cos^2\Lambda_R \tan^2\gamma_R}} -$$

$$\frac{h_F \cos \Lambda_F P_{x_F} L_F}{L_F \sqrt{1 + \cos^2\Lambda_R \tan^2\gamma_R}} + \frac{h_F \cos \gamma_F \sin \Lambda_F P_{y_F} L_F}{L_F \sqrt{1 + \cos^2\Lambda_F \tan^2\gamma_F}} - \frac{h_F \sin \gamma_F P_{z_F} L_F}{L_F} +$$

$$\frac{h_R \cos \Lambda_R P_{x_R} L_R}{L_R \sqrt{1 + \cos^2\Lambda_R \tan^2\gamma_R}} + \frac{h_R \cos \gamma_R \sin \Lambda_R P_{y_R} L_R}{L_R \sqrt{1 + \cos^2\Lambda_R \tan^2\gamma_R}} - \frac{h_R \sin \gamma_R P_{z_R} L_R}{L_R} = 0 \qquad (9)$$

for the yawing moments,

$$\phi_5 = \frac{\cos \Lambda_F \tan \gamma_F M_{x_F}}{\sqrt{1 + \cos^2\Lambda_F \tan^2\gamma_F}} - \frac{\sin \gamma_F \sin \Lambda_F M_{y_F}}{\sqrt{1 + \cos^2\Lambda_F \tan^2\gamma_F}} + \cos \gamma_F M_{z_F} -$$

$$\frac{\cos \Lambda_R \tan \gamma_R M_{x_R}}{\sqrt{1 + \cos^2\Lambda_R \tan^2\gamma_R}} - \frac{\sin \gamma_R \sin \Lambda_R M_{y_R}}{\sqrt{1 + \cos^2\Lambda_R \tan^2\gamma_R}} + \cos \gamma_R M_{z_R} = 0 \qquad (10)$$

and for the pitching moments,

$$\phi_6 = \frac{\cos \Lambda_F M_{x_F}}{\sqrt{1 + \cos^2\Lambda_F \tan^2\gamma_F}} - \frac{\cos \gamma_F \sin \Lambda_F M_{y_F}}{\sqrt{1 + \cos^2\Lambda_F \tan^2\gamma_F}} - \sin \gamma_F M_{z_F} +$$

$$\frac{\cos \Lambda_R M_{x_R}}{\sqrt{1 + \cos^2\Lambda_R \tan^2\gamma_R}} + \frac{\cos \gamma_R \sin \Lambda_R M_{y_R}}{\sqrt{1 + \cos^2\Lambda_R \tan^2\gamma_R}} + \sin \gamma_R M_{z_R} +$$

$$\frac{h_F \sin \Lambda_F P_{x_F} L_F}{L_F\sqrt{1 + \cos^2\Lambda_F \tan^2\gamma_F}} + \frac{h_F \cos \Lambda_F P_{y_F} L_F}{L_F \cos \gamma_F \sqrt{1 + \cos^2\Lambda_F \tan^2\gamma_F}} +$$

$$\frac{h_R \sin \Lambda_R P_{x_R} L_R}{L_R\sqrt{1 + \cos^2\Lambda_R \tan^2\gamma_R}} - \frac{h_R \cos \Lambda_R P_{y_R} L_R}{L_R \cos \gamma_R \sqrt{1 + \cos^2\Lambda_R \tan^2\gamma_R}} = 0 \qquad (11)$$

It is desired to minimize the total strain energy, equation (5), with the condition that equations (6) to (11) be satisfied. In order to do this, it is sufficient to set

$$\delta\left(\text{S.E.} + \sum_{i=1}^{i=6} \lambda_i \phi_i\right) = 0 \qquad (12)$$

where the λ's are Lagrangian multipliers (ref. 4). Substituting equations (5) to (11) into equation (12) and setting the variation equal to zero results in 18 linear simultaneous equations. The 18 equations obtained for the swept biplane model of figure 2 subjected to the elliptically distributed lift load of 20.03 pounds are given in matrix form in table IX. The first 12 equations in table IX have been multiplied by the constant E for convenience of computation. The equations may be solved by a numerical process; the particular method used in this instance is that given by reference 5.

The eighteen equations obtained for the swept biplane model subjected to the unit torque loading as shown in figure 5 are identical to the

equations shown in table IX except for the loading constants on the right-hand side of the equations; these constants are all zero with the exception of the fourth term which is

$$-\int_0^{L_F} T \frac{Ed_x}{GJ_y} - \frac{c_F ET \sin^3\Lambda_F \cos^2\Lambda_F}{2I_{y_F}} = -2220 - 97 = -2317$$

The resulting values of the forces and moments at the cut sections are given in table VII for the elliptically distributed load of 20.03 pounds and in table VIII for the unit torque load. With these forces and moments known, the stresses and the deflections of the front and rear beams can be readily calculated by elementary theory.

REFERENCES

1. Cahill, Jones F., and Stead, Dexter H.: Preliminary Investigation at Subsonic and Transonic Speeds of the Aerodynamic Characteristics of a Biplane Composed of a Sweptback and a Sweptforward Wing Joined at the Tips. NACA RM L53L24b, 1954.

2. Zender, George W., and Brooks, William A., Jr.: An Approximate Method of Calculating the Deformations of Wings Having Swept, M or W, Λ, and Swept-Tip Plan Forms. NACA TN 2978, 1953.

3. Reissner, Eric, and Stein, Manuel: Torsion and Transverse Bending of Cantilever Plates. NACA TN 2369, 1951.

4. Sokolnikoff, Ivan S., and Sokolnikoff, Elizabeth S.: Higher Mathematics for Engineers and Physicists. Second ed., McGraw-Hill Book Co., Inc., 1941, pp. 163-167.

5. Crout, Prescott D.: A Short Method for Evaluating Determinants and Solving Systems of Linear Equations With Real or Complex Coefficients. Trans. Am. Inst. Elec. Eng., vol. 60, 1941, pp. 1235-1240.

TABLE I.- DEFLECTIONS FOR CONCENTRATED LIFT LOADS

n	$w_{n_F}(\xi)$, in./lb						$w_{n_R}(\xi)$, in./lb					
	ξ = 5.5 in.	ξ = 7.5 in.	ξ = 9.5 in.	ξ = 11.5 in.	ξ = 13.5 in.	ξ = 15.5 in.	ξ = 5.5 in.	ξ = 7.5 in.	ξ = 9.5 in.	ξ = 11.5 in.	ξ = 13.5 in.	ξ = 15.5 in.
1	0.063×10^{-4}	0.076×10^{-4}	0.064×10^{-4}	0.064×10^{-4}	0.074×10^{-4}	0.073×10^{-4}	0×10^{-4}	0×10^{-4}	0×10^{-4}	0×10^{-4}	0.030×10^{-4}	0.061×10^{-4}
2	.758	.983	.957	.949	.740	.521	.130	.182	.268	.360	.412	.391
3	1.311	1.549	1.563	1.453	1.311	1.140	.061	.133	.244	.398	.601	.754
4	-----	4.557	4.663	5.000	4.346	3.200	.619	1.075	1.535	1.965	2.332	2.384
5	3.298	4.452	5.430	4.787	4.122	3.500	.384	.728	1.030	1.507	2.035	2.301
6	3.990	6.745	8.693	8.964	8.243	6.500	1.244	2.097	3.341	4.013	4.704	5.044
7	4.040	6.432	8.098	9.325	7.673	6.330	.808	1.413	2.241	3.216	4.049	4.424
8	3.739	7.067	9.742	11.009	10.913	9.200	1.808	3.125	4.663	5.959	7.133	7.483
9	3.541	6.371	8.617	9.742	9.913	8.680	1.238	2.174	3.310	4.663	6.009	7.075
10	2.868	5.543	7.954	9.573	10.630	10.400	2.174	3.839	5.553	7.332	8.693	9.244
11	2.633	4.877	6.809	8.541	9.629	9.610	1.458	2.603	3.837	5.373	7.002	8.391
12	2.279	3.990	5.891	7.813	9.163	8.750	3.064	5.095	7.133	9.004	10.088	10.000
13	1.649	3.373	5.095	6.809	8.170	9.090	2.772	4.502	6.494	8.243	9.913	10.818
14	1.919	3.566	5.261	6.619	7.604	7.260	4.271	6.757	8.847	10.176	9.827	8.770
15	1.434	3.034	4.400	5.832	6.619	7.640	4.122	6.494	8.693	9.742	9.742	9.004
16	1.293	2.466	3.640	4.452	5.133	4.875	4.582	7.133	8.391	8.243	7.445	6.371
17	.099	2.046	3.057	3.201	4.463	5.260	4.663	6.969	8.490	8.170	7.332	6.068
18	.650	1.250	1.769	2.226	2.583	2.380	3.633	4.636	4.770	4.452	3.837	3.655
19	.477	.954	1.375	1.833	2.145	2.500	3.526	4.871	5.068	5.040	3.872	3.685
20	.160	.315	.404	.526	.600	.568	1.063	1.250	1.250	1.111	.949	.788
21	.127	.249	.344	.456	.532	.676	1.507	1.678	1.563	1.303	1.150	.832
22	0	0	0	0	0	0	.096	.078	.057	.047	0	0

TABLE II. - STRESSES FOR CONCENTRATED LIFT LOADS

[Tensile stresses positive]

n	$\sigma_{n_F}(\xi)$						$\sigma_{n_R}(\xi)$					
	ξ = 5.5 in.	ξ = 7.5 in.	ξ = 9.5 in.	ξ = 11.5 in.	ξ = 13.5 in.	ξ = 15.5 in.	ξ = 5.5 in.	ξ = 7.5 in.	ξ = 9.5 in.	ξ = 11.5 in.	ξ = 13.5 in.	ξ = 15.5 in.
1	-28.0	-35.1	-32.2	-23.5	-9.2	8.4	0.5	0	2.0	3.5	7.9	15.1
2	-78.0	-101.8	-114.7	-116.7	-110.0	-96.2	-17.3	-30.4	-44.7	-60.5	-71.7	-76.0
3	33.1	16.1	5.3	2.2	5.4	13.4	1.3	1.5	3.8	5.8	10.0	15.4
4	23.4	-2.6	-24.7	-40.1	-50.8	-55.0	-8.6	-17.2	-26.1	-35.9	-44.6	-53.4
5	31.0	60.2	59.8	43.1	31.8	26.8	5.4	7.2	11.3	14.6	19.1	22.5
6	25.2	51.9	43.0	19.4	-1.7	-15.6	-3.6	-7.4	-10.7	-15.1	-19.1	-25.0
7	17.9	37.5	64.5	81.2	58.8	40.9	7.5	11.6	17.3	21.9	27.1	29.1
8	14.2	32.5	56.2	72.5	41.9	15.1	-.1	-.7	-.5	-.9	-1.4	-4.2
9	3.5	10.8	21.7	38.6	62.0	52.0	9.5	14.8	21.0	26.2	31.3	33.1
10	3.6	10.9	22.3	38.2	60.2	42.2	3.9	6.3	9.7	11.9	14.3	13.5
11	-6.2	-9.9	-14.4	-15.7	-14.5	-8.1	-43.3	-52.0	-48.7	-37.5	-24.8	-10.9
12	-8.6	-17.5	-25.0	-35.1	-44.2	-50.6	-41.1	-60.5	-69.0	-71.6	-69.4	-64.0
13	-.6	-1.2	-1.2	.4	3.2	8.4	37.1	19.0	7.1	3.7	5.0	10.0
14	-5.4	-9.6	-15.6	-22.6	-29.3	-33.4	28.5	2.1	-18.0	-30.3	-36.6	-38.3
15	2.3	5.3	7.8	10.0	13.0	16.5	38.1	64.2	55.6	36.8	26.0	21.1
16	-1.7	-2.9	-5.0	-8.6	-12.3	-14.8	31.9	56.0	42.2	17.3	0	-11.1
17	6.3	11.1	16.6	21.2	23.3	25.6	20.5	38.7	66.4	73.6	51.1	33.4
18	2.0	4.7	5.6	6.0	4.7	3.6	18.5	35.5	59.6	67.4	39.2	16.6
19	8.4	17.9	26.4	33.0	36.8	37.6	6.7	13.6	27.2	44.8	66.4	52.0
20	5.1	11.5	17.3	21.2	23.5	24.5	6.2	12.5	25.2	42.0	63.9	46.4
21	41.8	60.6	71.1	73.6	71.6	68.1	11.3	18.5	28.4	37.7	47.3	54.9
22	72.6	90.4	90.3	77.6	53.6	23.2	6.3	9.1	13.5	15.8	15.2	5.6
23	-24.7	1.5	22.0	34.1	41.5	48.1	9.4	14.3	22.3	29.6	38.2	45.7
24	-20.3	-6.9	0	1.1	.5	-3.2	0	-1.4	-2.3	-2.4	-5.2	-8.0
25	-24.2	-46.0	-35.5	-13.1	4.5	19.9	6.1	8.2	12.2	15.9	20.8	26.8
26	-35.2	-64.8	-59.4	-43.1	-34.2	-27.3	-3.2	-7.4	-11.5	-16.0	-19.1	-21.7
27	-13.9	-28.4	-49.0	-61.9	-34.9	-4.9	1.4	.2	.4	.8	2.3	7.2
28	-19.9	-39.1	-67.6	-86.2	-65.0	-45.9	-6.6	-13.1	-19.7	-26.2	-31.3	-31.4
29	-3.2	-8.7	-18.1	-33.1	-55.0	-39.4	-2.6	-6.6	-9.8	-12.0	-13.4	-12.8
30	-5.4	-11.5	-22.6	-40.8	-67.7	-55.4	-9.5	-18.0	-26.7	-32.8	-36.3	-38.5
31	11.2	21.3	33.9	43.6	53.0	59.6	62.4	80.8	86.3	84.2	78.4	72.9
32	3.6	7.5	10.0	12.2	11.4	4.4	28.9	36.7	38.8	31.7	23.3	13.0
33	5.7	10.8	17.5	23.4	29.3	35.0	-26.9	2.8	16.8	29.2	36.0	40.0
34	1.5	2.6	3.6	2.9	.6	-1.2	-35.5	-17.6	-4.4	-.5	.5	-1.5
35	2.0	4.8	8.0	11.1	14.6	18.0	-27.9	-49.9	-36.8	-11.9	4.3	14.6
36	-2.7	-3.8	-6.3	-8.1	-11.4	-13.0	-34.0	-63.6	-56.5	-38.5	25.9	-19.0
37	-1.5	-2.3	-2.9	-2.7	-1.4	1.9	-15.6	-30.5	-52.2	-56.0	-30.6	-12.0
38	-5.6	-9.7	-13.8	-19.2	-22.8	-23.2	-18.5	-37.4	-64.6	-74.4	-51.6	-33.0
39	-5.0	-8.7	-13.2	-15.4	-17.0	-14.9	-5.1	-13.6	-24.3	-39.4	-56.2	-37.3
40	-8.1	-14.4	-22.5	-28.0	-33.2	-32.3	-3.8	-12.1	-24.4	-40.9	-61.4	-46.9
41	-16.7	-19.8	23.4	29.4	33.6	36.6	1.6	2.5	5.9	12.7	23.0	30.4
42	-7.1	-13.2	-19.5	-23.5	-24.8	-10.9	11.4	15.8	20.8	18.9	16.4	11.5
43	36.0	43.0	44.2	40.5	35.8	29.5	4.3	5.6	9.2	12.7	17.4	21.0
44	10.0	25.8	30.1	27.9	21.1	2.3	-17.4	-28.2	-38.2	-41.2	-41.1	-37.3

TABLE III.- EXPERIMENTAL DEFLECTIONS FOR 20.03-POUND LIFT LOAD ELLIPTICALLY DISTRIBUTED

n	w_{n_F}, in.	w_{n_R}, in.	w_n, in.
1	0.72×10^{-4}	0.06×10^{-4}	0.78×10^{-4}
2	9.10	1.22	10.32
3	14.84	1.36	16.20
4	45.70	6.84	52.54
5	43.30	4.90	48.20
6	65.20	14.45	79.65
7	65.20	11.10	76.30
8	77.40	21.60	99.00
9	69.65	16.45	86.10
10	69.00	25.50	94.50
11	58.70	19.35	78.05
12	52.90	30.65	83.55
13	45.80	35.80	81.60
14	45.15	37.40	82.55
15	39.35	36.10	75.45
16	30.70	32.60	63.30
17	25.30	33.20	58.50
18	15.48	22.55	38.03
19	12.38	23.85	36.23
20	3.49	6.00	9.49
21	3.03	7.87	10.90
22	0	.33	.33

TABLE IV.- EXPERIMENTAL STRESSES FOR 20.03-POUND LIFT LOAD ELLIPTICALLY DISTRIBUTED

[Tensile stresses positive]

n	σ_{n_F}, psi	σ_{n_R}, psi	σ_n, psi	n	σ_{n_F}, psi	σ_{n_R}, psi	σ_n, psi
1	-262	18	-244	23	53	113	166
2	-1050	-207	-1257	24	-119	-12	-131
3	197	23	220	25	-202	67	-135
4	-112	-126	-238	26	-438	-54	-492
5	415	57	472	27	-311	9	-302
6	248	-55	193	28	-485	-89	-574
7	451	84	535	29	-201	-40	-241
8	356	-5	351	30	-263	-115	-378
9	244	100	344	31	307	379	686
10	232	44	276	32	77	163	240
11	-112	-220	-332	33	164	6	170
12	-246	-286	-532	34	20	-112	-92
13	6	110	116	35	79	-111	-32
14	-155	-13	-168	36	-62	-196	258
15	73	202	275	37	-18	-157	-175
16	-59	141	82	38	-132	-200	-332
17	146	227	373	39	-109	-117	-226
18	42	195	237	40	-196	-123	-319
19	223	141	364	41	254	45	299
20	144	132	276	42	-152	81	-71
21	624	140	764	43	420	102	522
22	796	55	851	44	200	-155	45

TABLE V.- EXPERIMENTAL DEFLECTIONS

FOR UNIT TORQUE LOAD

n	w_n, in.
1	-3.4×10^{-6}
2	-26.7
3	0
4	-46.1
5	-33.3
6	-8.0
7	-17.8
8	-16.0

TABLE VI.- EXPERIMENTAL STRESSES

FOR UNIT TORQUE LOAD

[Tensile stresses positive]

n	σ_n, psi	n	σ_n, psi
1	3.969	23	2.106
2	1.812	24	-1.350
3	2.058	25	2.922
4	-1.389	26	.686
5	-4.875	27	2.904
6	-2.676	28	3.048
7	-2.205	29	.918
8	-2.709	30	5.784
9	-.867	31	0
10	-3.117	32	-2.550
11	3.534	33	1.749
12	0	34	1.497
13	1.970	35	2.886
14	-1.272	36	0
15	.645	37	5.716
16	-2.658	38	1.626
17	-.933	39	6.495
18	-4.395	40	4.083
19	-3.189	41	2.451
20	-6.582	42	5.940
21	1.098	43	0
22	-6.900	44	1.626

TABLE VII.- FORCES AND MOMENTS AT CUT SECTIONS FOR 20.03-POUND LIFT LOAD ELLIPTICALLY DISTRIBUTED

Front wing:	
P_{x_F}, lb	-7.230
P_{y_F}, lb	10.028
P_{z_F}, lb	-3.204
M_{x_F}, lb-in.	-6.362
M_{y_F}, lb-in.	-0.704
M_{z_F}, lb-in.	-19.934
Rear wing:	
P_{x_R}, lb	10.397
P_{y_R}, lb	7.370
P_{z_R}, lb	-0.837
M_{x_R}, lb-in.	3.549
M_{y_R}, lb-in.	-10.636
M_{z_R}, lb-in.	19.786

TABLE VIII.- FORCES AND MOMENTS AT CUT SECTIONS

FOR UNIT TORQUE LOAD

Front wing:	
P_{x_F}, lb	0.019
P_{y_F}, lb	0.162
P_{z_F}, lb	-0.013
M_{x_F}, lb-in.	-0.768
M_{y_F}, lb-in.	0.223
M_{z_F}, lb-in.	-1.172
Rear wing:	
P_{x_R}, lb	0.161
P_{y_R}, lb	-0.021
P_{z_R}, lb	-0.020
M_{x_R}, lb-in.	-0.081
M_{y_R}, lb-in.	0.285
M_{z_R}, lb-in.	1.310

TABLE IX.- SYSTEM OF 18 EQUATIONS FOR SWEPT BIPLANE WITH 20.03-POUND LIFT LOAD ELLIPTICALLY DISTRIBUTED

.0423	0	0	0	0	0	0	0	0	0	0	0	.7025	.1146	.7025	-.0192	0	.0192	$P_{x_F}l_F$	0.5320
0	4.2912	0	0	0	6.4368	0	0	0	0	0	0	-.6933	-.1131	.7117	.0189	0	.0194	$P_{y_F}l_F$	-53.096
0	0	1452.0	107.66	2113.3	0	0	0	0	0	0	0	.1610	-.9870	0	-.0044	0	0	$P_{z_F}l_F$	-111107
0	0	107.66	2668.1	100.90	0	0	0	0	0	0	0	0	0	0	.7025	.1146	.7025	M_{x_F}	-12431
0	0	2113.3	100.90	4112.2	0	0	0	0	0	0	0	0	0	0	.7117	-.1131	-.6933	M_{y_F}	-139147
0	6.4368	0	0	0	12.874	0	0	0	0	0	0	0	0	0	0	.9870	-.1610	M_{z_F}	-68.596
0	0	0	0	0	0	.0423	0	0	0	0	0	.7025	-.1146	-.7025	.0192	0	.0192	$P_{x_R}l_R$	-.2660
0	0	0	0	0	0	0	4.2912	0	0	0	6.4368	.6933	-.1131	.7117	.0189	0	-.0194	$P_{y_R}l_R$	-26.548
0	0	0	0	0	0	0	0	1452.0	107.66	2113.3	0	-.1610	-.9870	0	-.0044	0	0	$P_{z_R}l_R$ =	-55.554
0	0	0	0	0	0	0	0	107.66	2668.1	100.90	0	0	0	0	-.7025	-.1146	.7025	M_{x_R}	-6215.5
0	0	0	0	0	0	0	0	2113.3	100.90	4112.2	0	0	0	0	.7117	-.1131	.6933	M_{y_R}	-69573
0	0	0	0	0	0	0	6.4368	0	0	0	12.874	0	0	0	0	.9870	.1610	M_{z_R}	-34.298
.7025	-.6933	.1610	0	0	0	.7025	.6933	-.1610	0	0	0	0	0	0	0	0	0	$\lambda_1 E$	0
.1146	-.1131	-.9870	0	0	0	-.1146	-.1131	-.9870	0	0	0	0	0	0	0	0	0	$\lambda_2 E$	0
.7025	.7117	0	0	0	0	-.7025	.7117	0	0	0	0	0	0	0	0	0	0	$\lambda_3 E$	0
-.0192	.0189	-.0044	.7025	.7117	0	.0192	.0189	-.0044	-.7025	.7117	0	0	0	0	0	0	0	$\lambda_4 E$	0
0	0	0	.1146	-.1131	.9870	0	0	0	-.1146	-.1131	.9870	0	0	0	0	0	0	$\lambda_5 E$	0
.0192	.0194	0	.7025	-.6933	-.1610	.0192	-.0194	0	.7025	.6933	.1610	0	0	0	0	0	0	$\lambda_6 E$	0

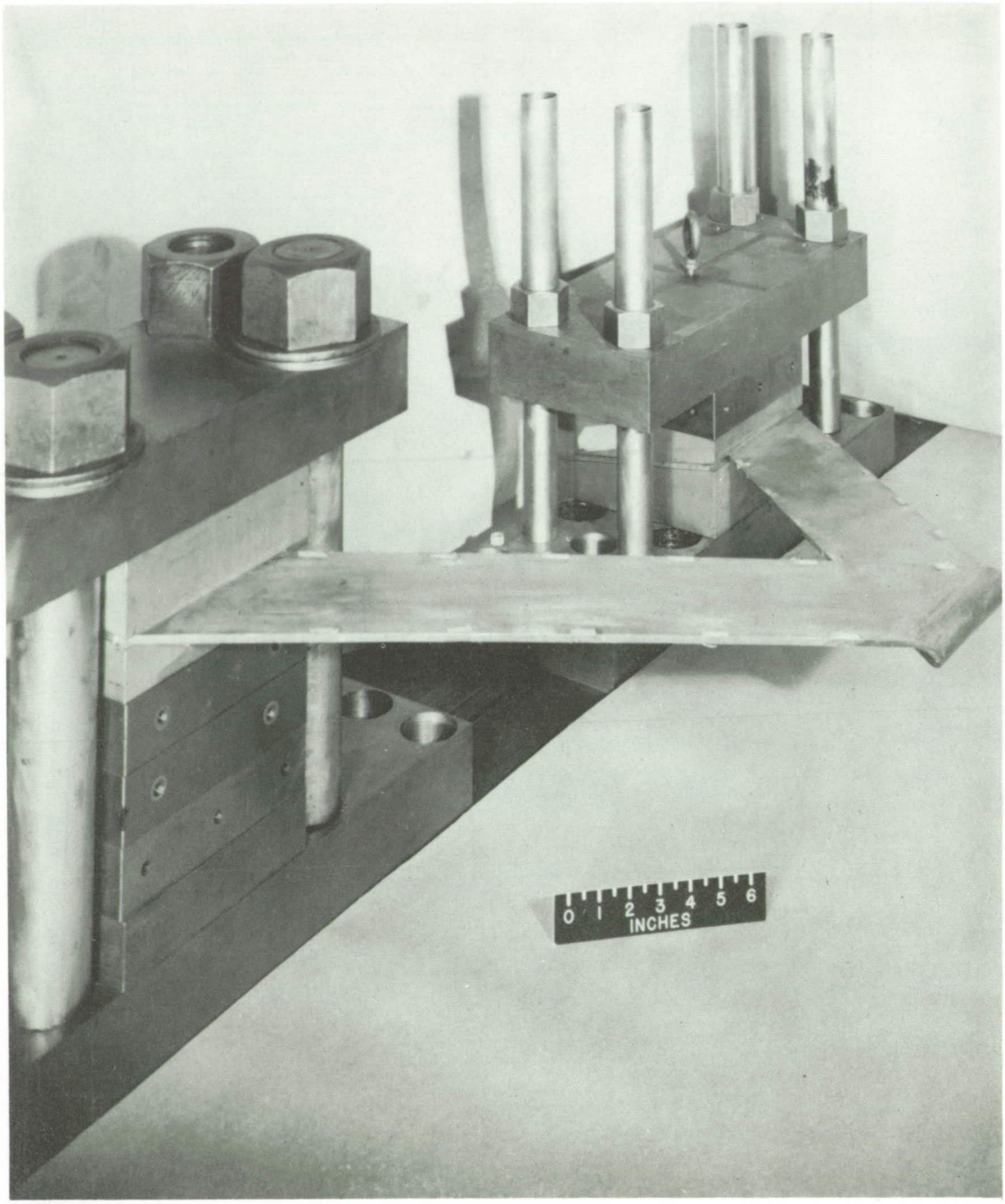

L-83917

Figure 1.- Test setup of swept biplane wing.

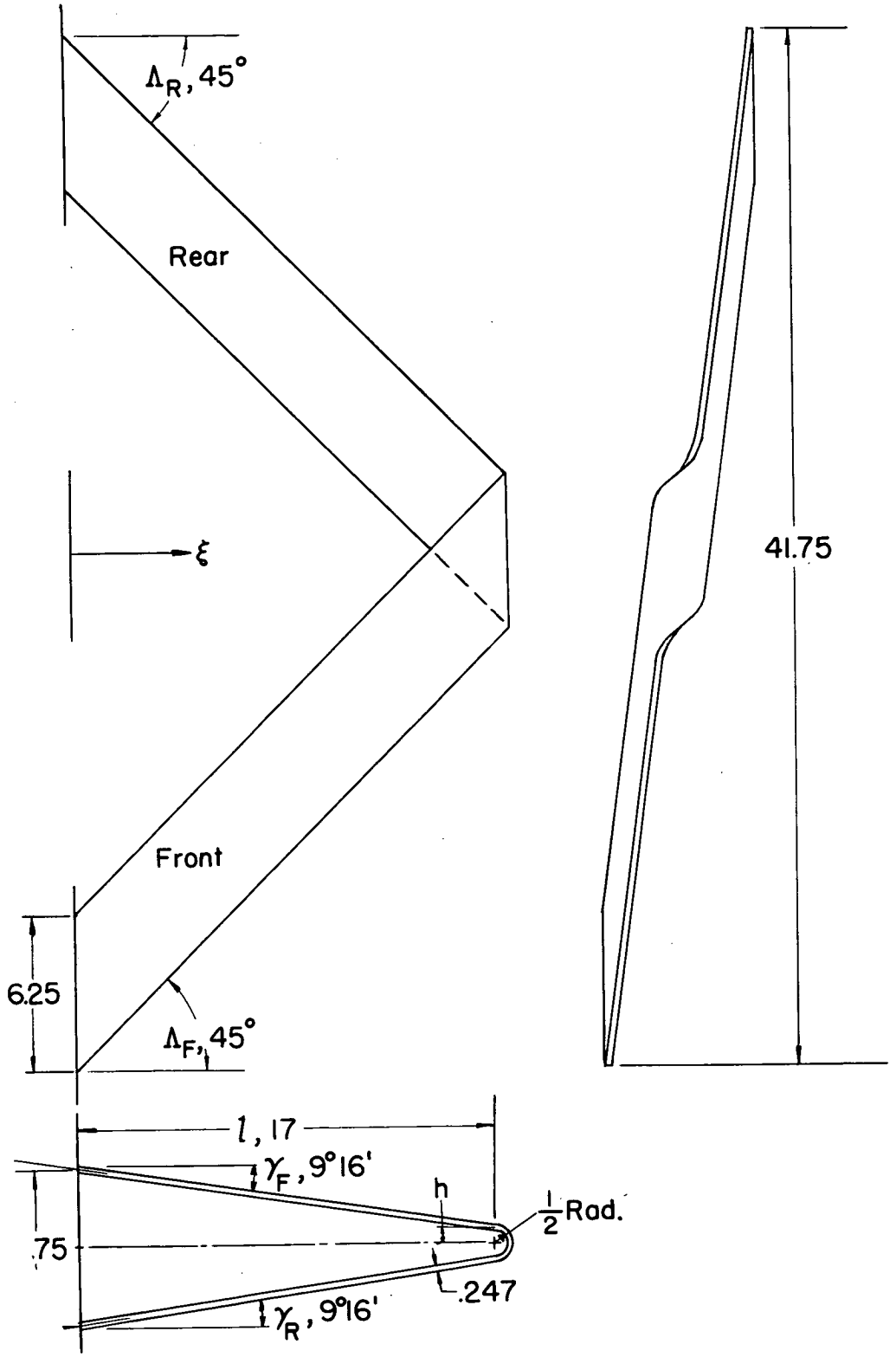

Figure 2.- Details of swept biplane wing.

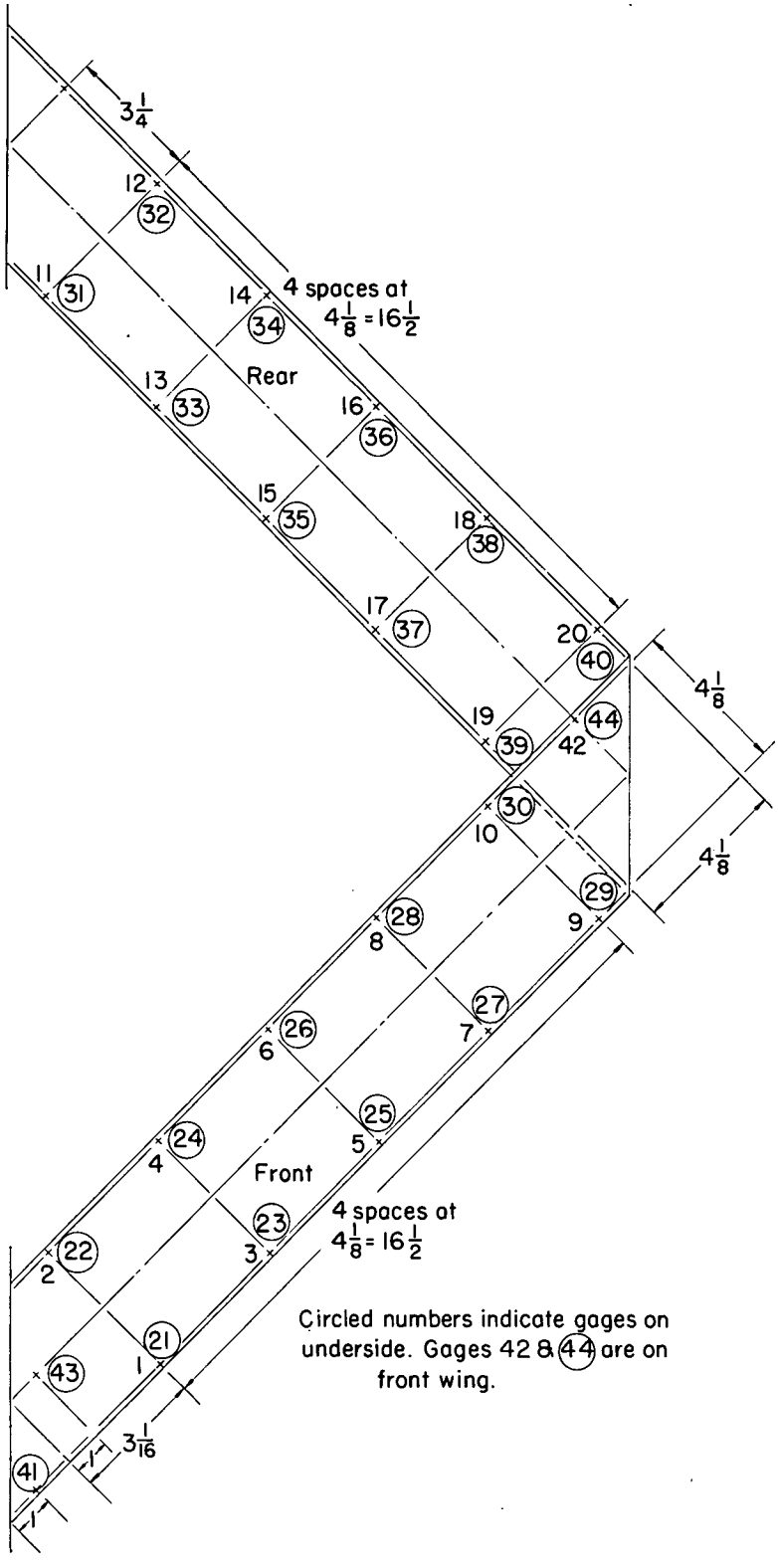

Figure 3.- Location of strain gages for lift and torque loads.

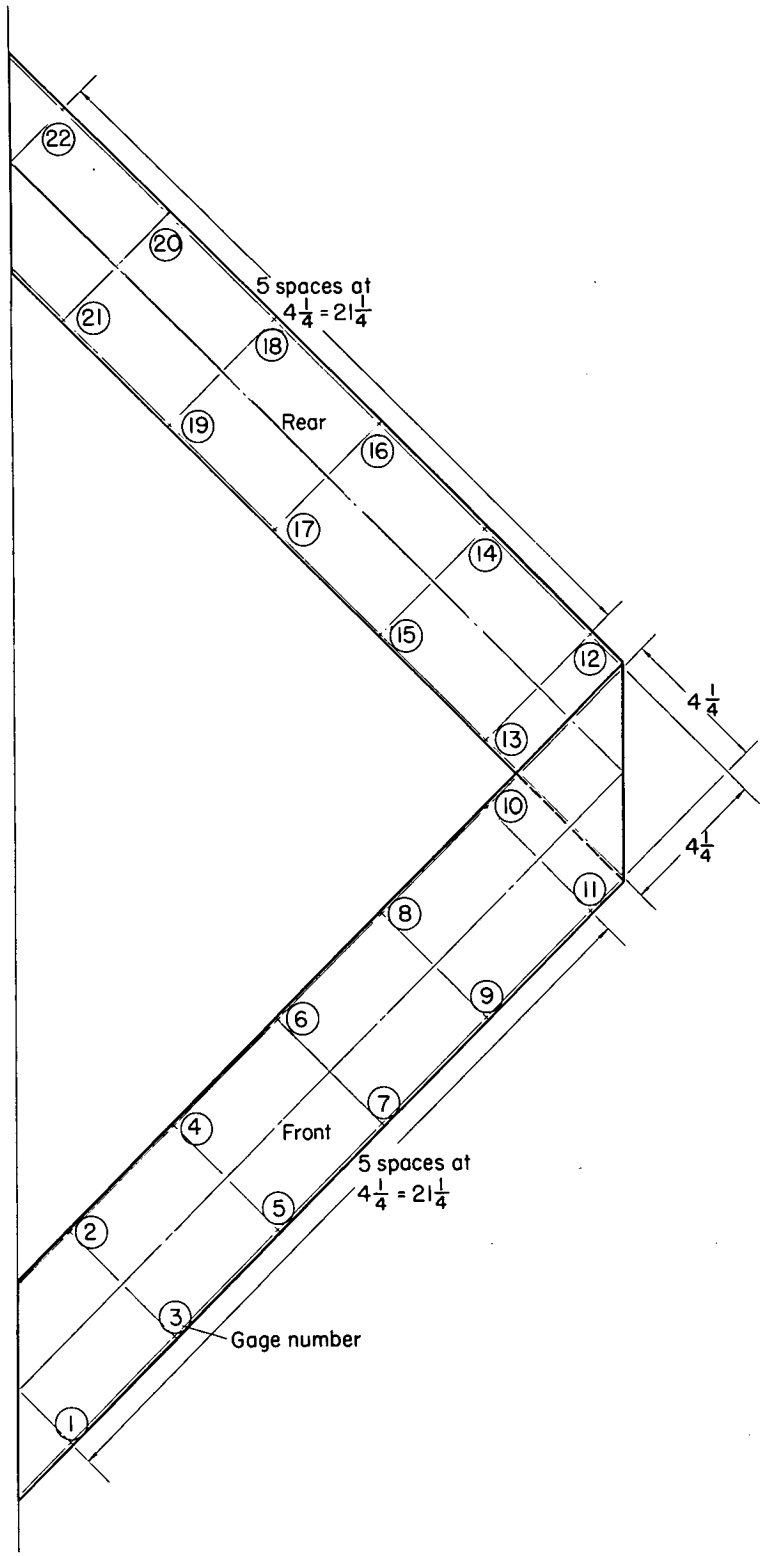

Figure 4.- Location of deflection gages for lift loads.

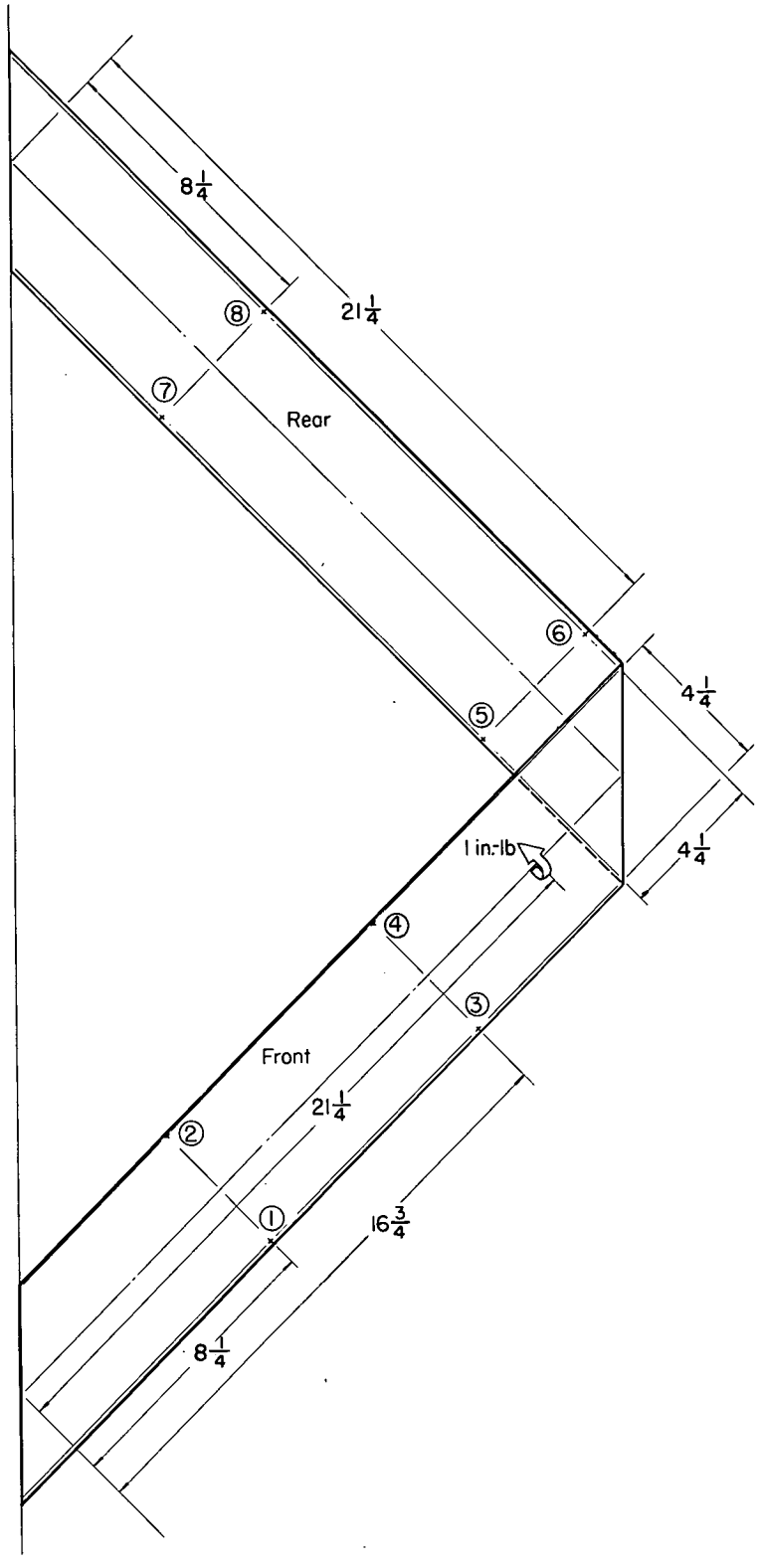

Figure 5.- Location of deflection gages for unit torque load.

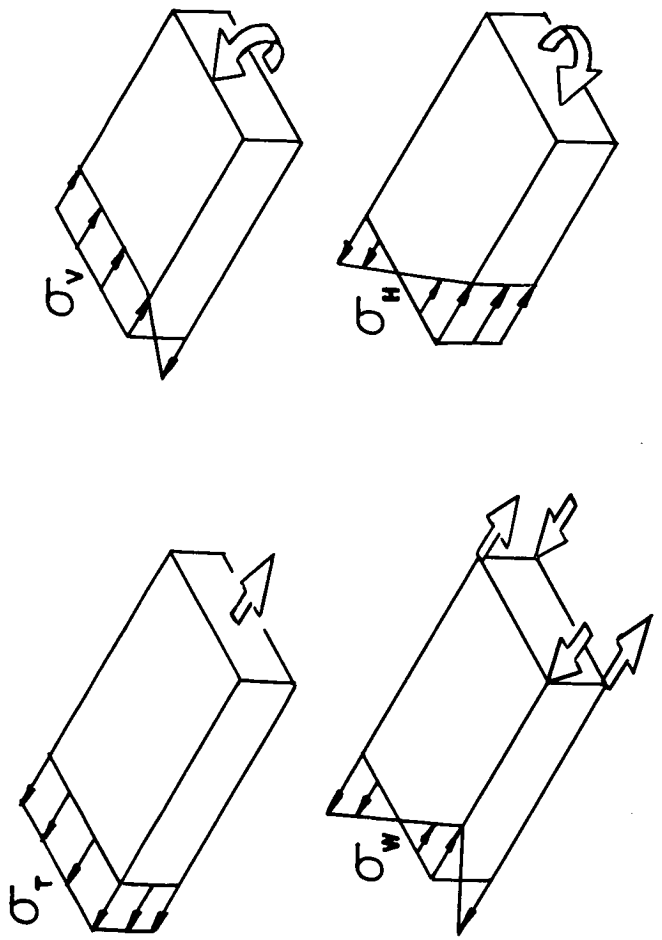

Figure 6. Four stress components assumed acting on biplane cross section.

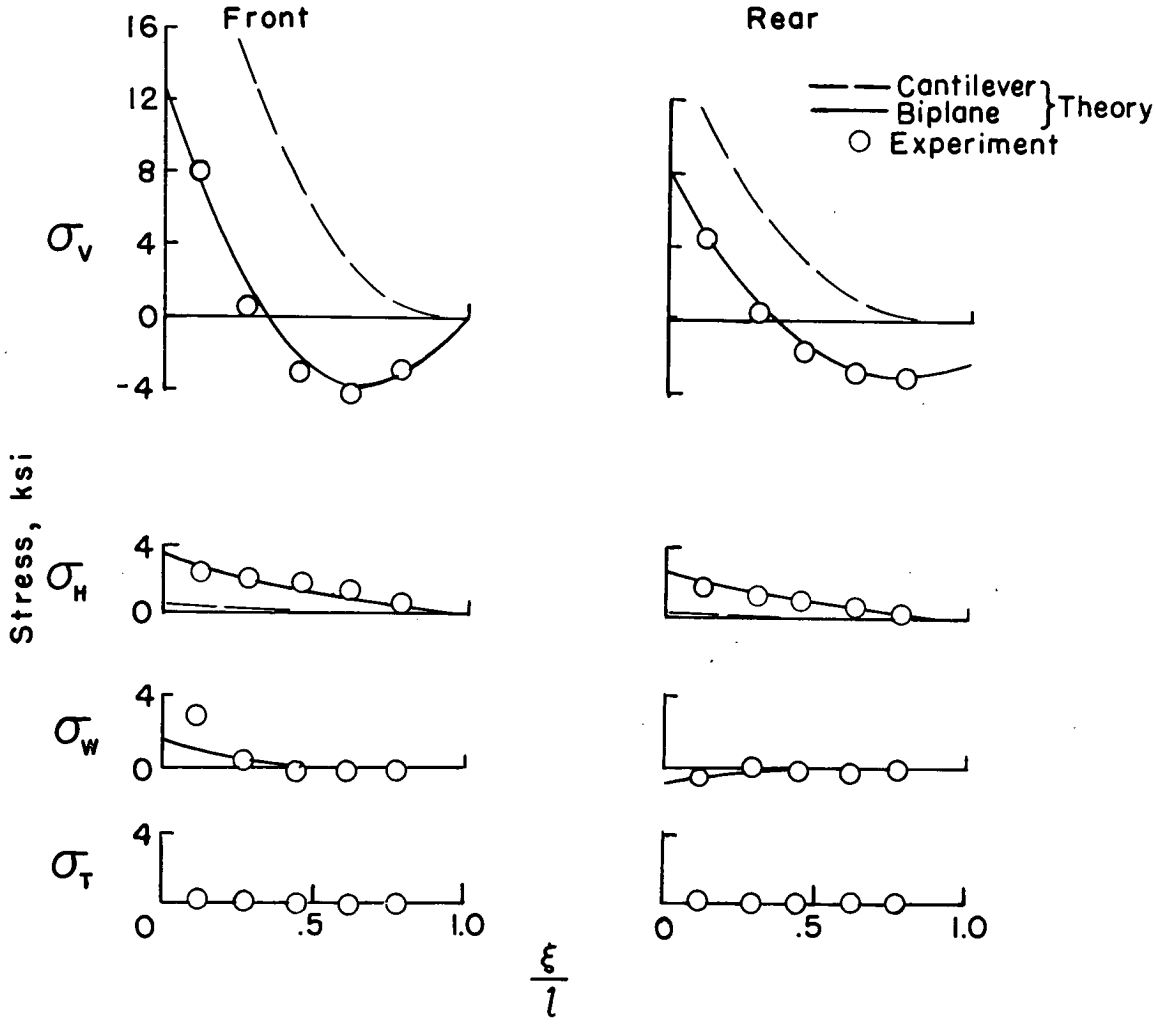

Figure 7.- Comparison of theoretical and experimental stress components for 20.03-pound lift load elliptically distributed.

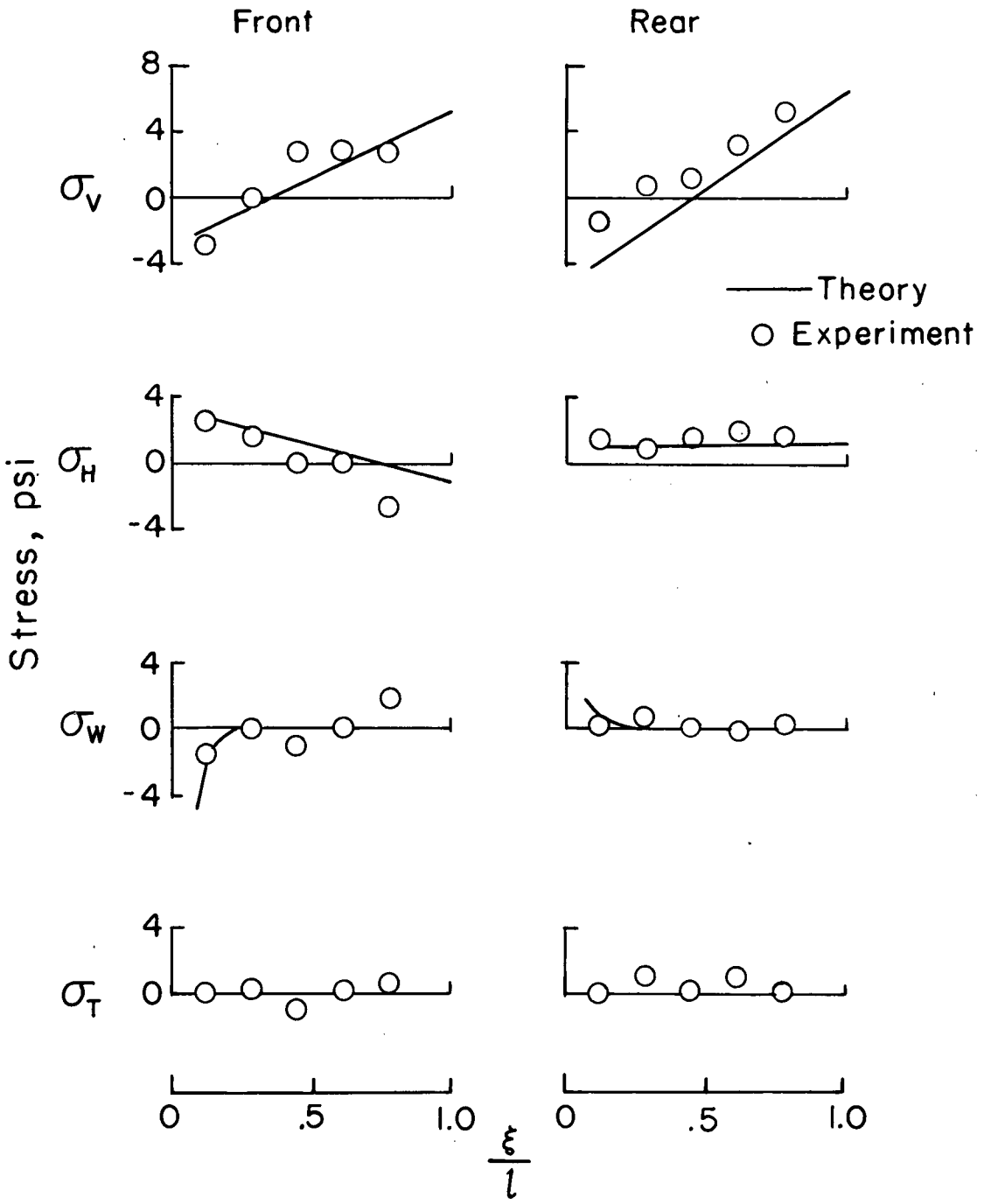

Figure 8.- Comparison of theoretical and experimental stress components for unit torque load.

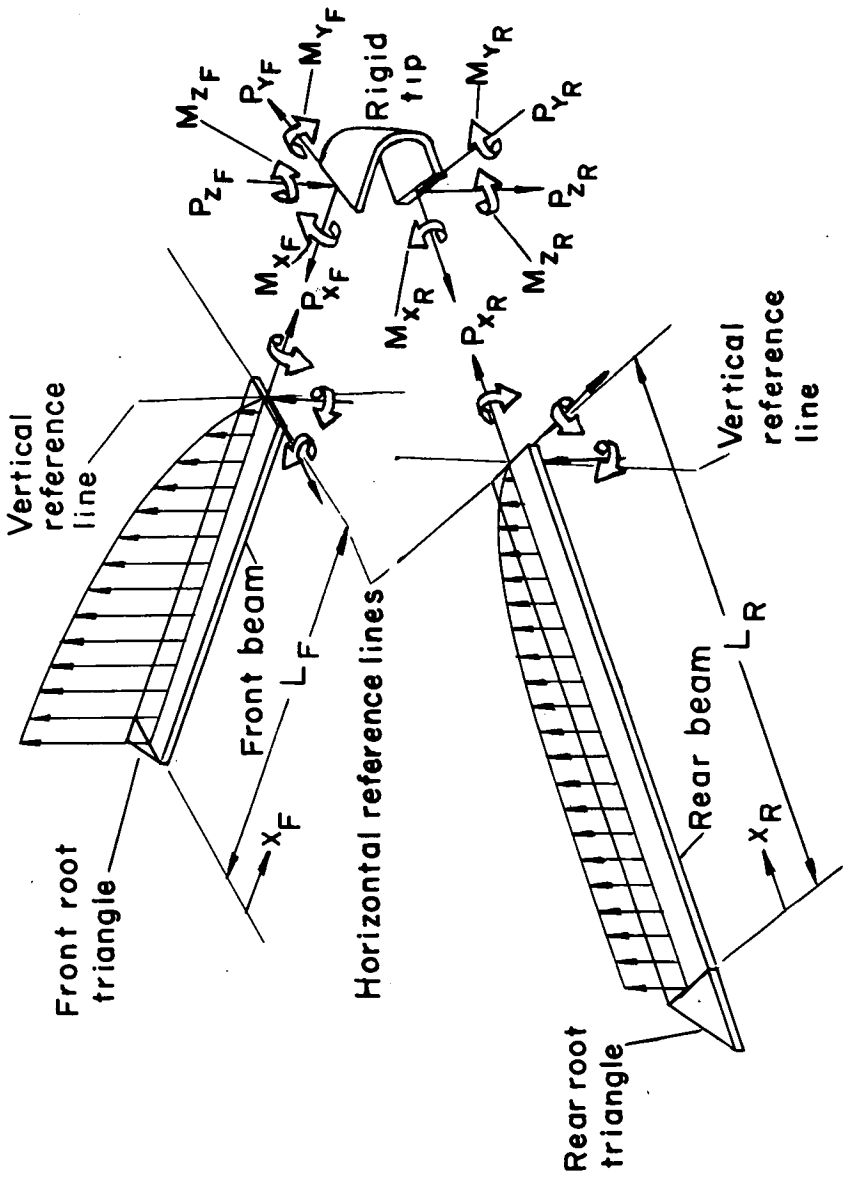

Figure 9.- Five component parts of biplane used in analysis.

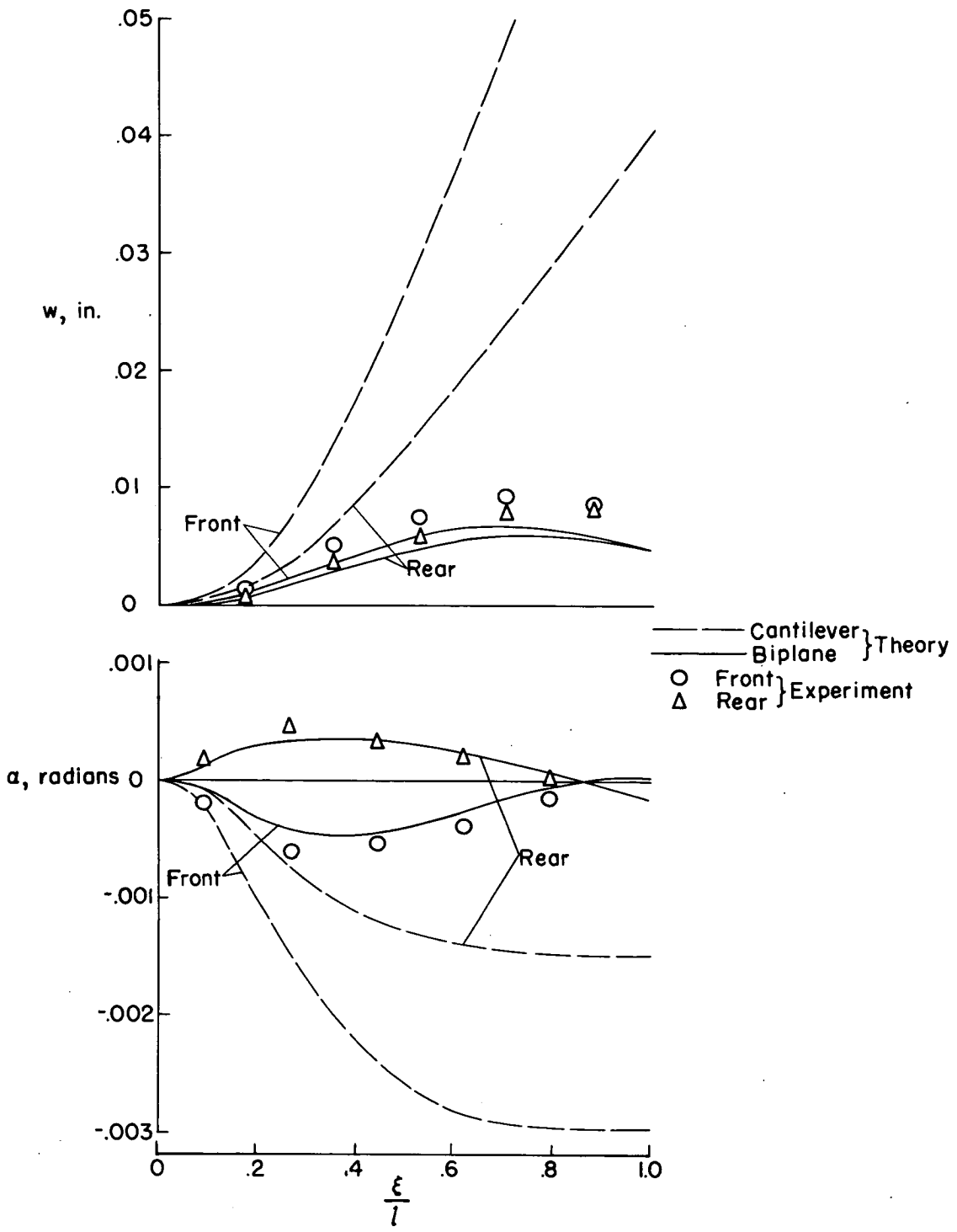

Figure 10.- Comparison of theoretical and experimental distortions for 20.03-pound lift load elliptically distributed.

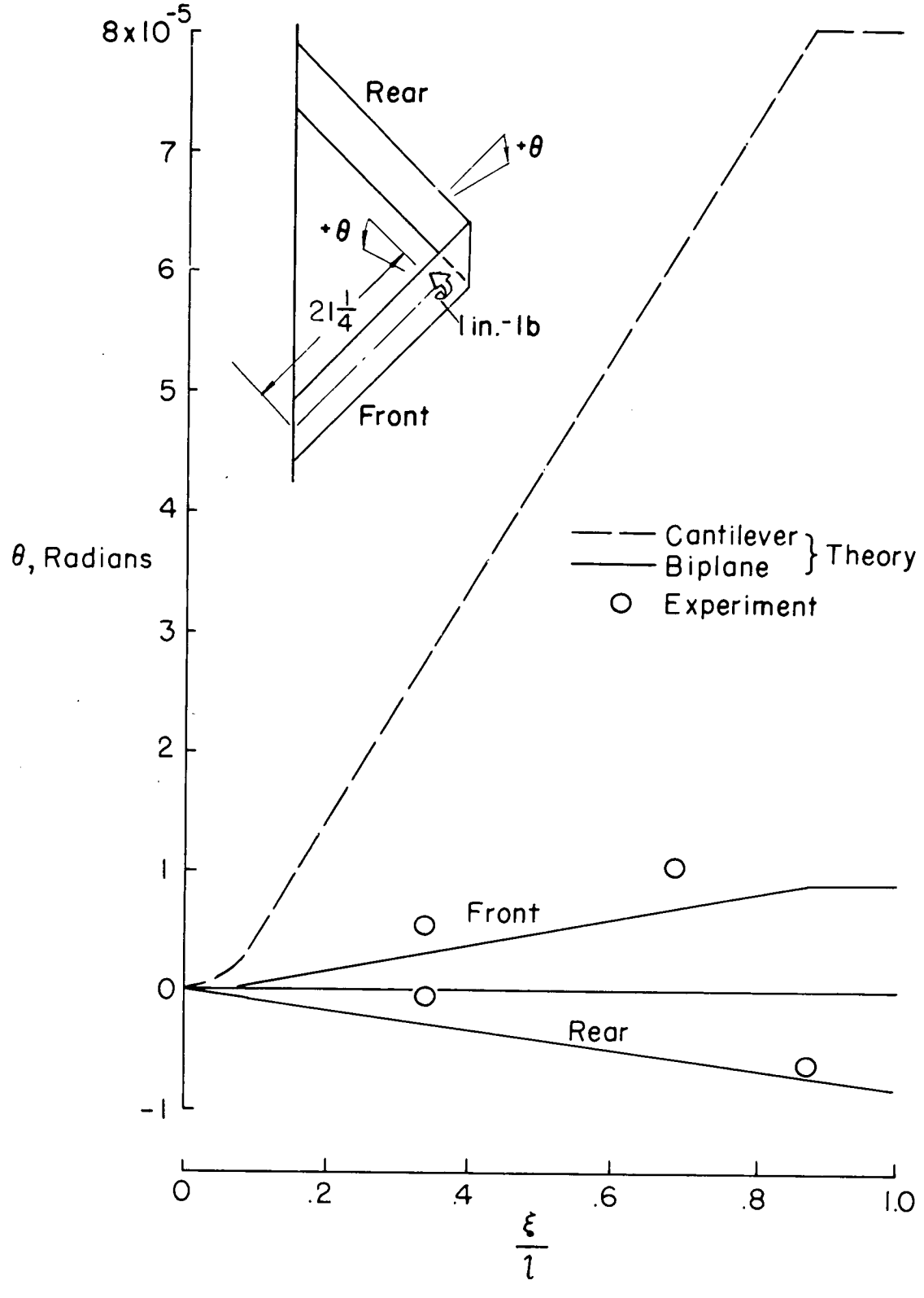

Figure 11.- Structural twist of swept biplane for unit torque load.

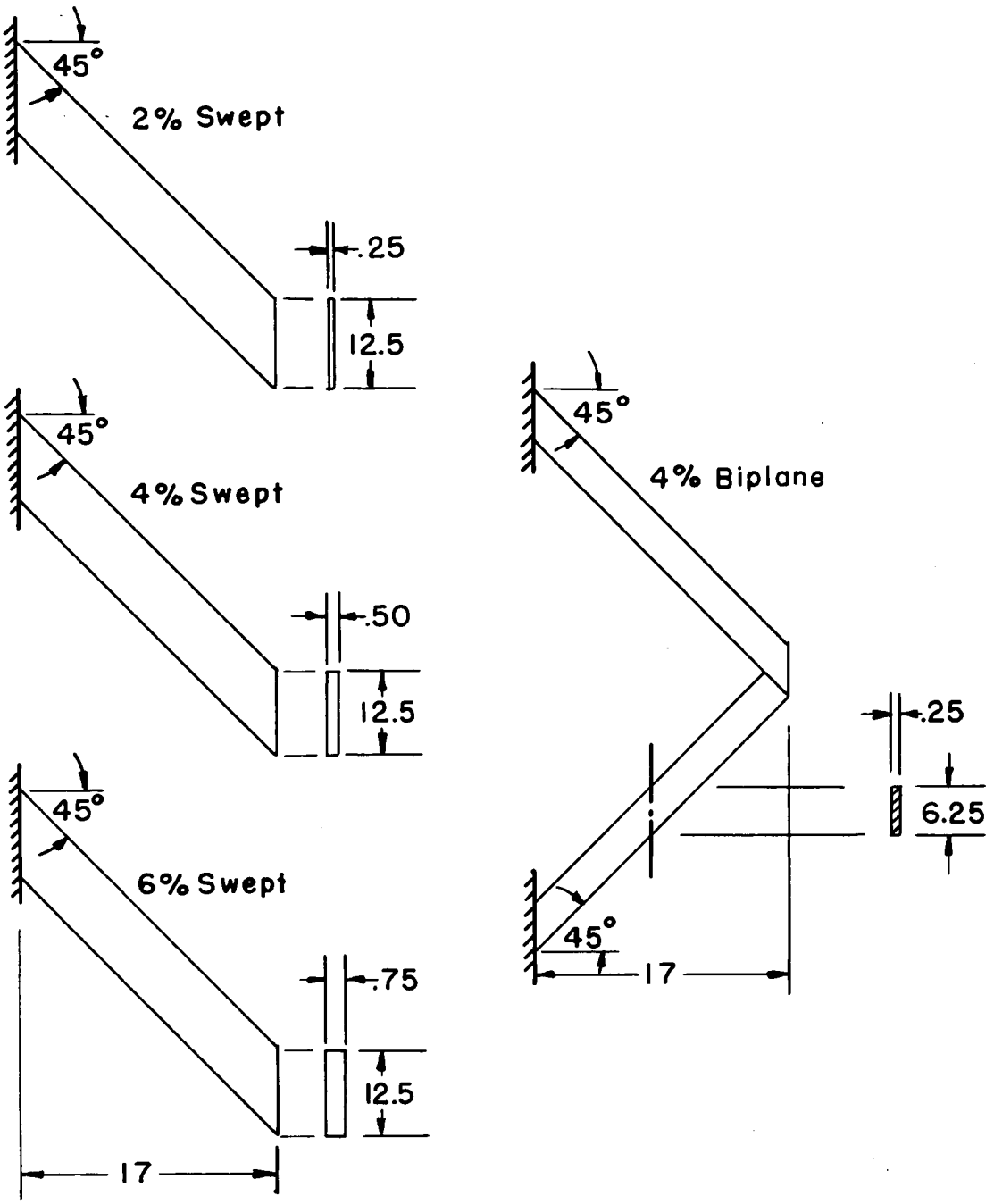

Figure 12.- Details of models used for structural comparisons.

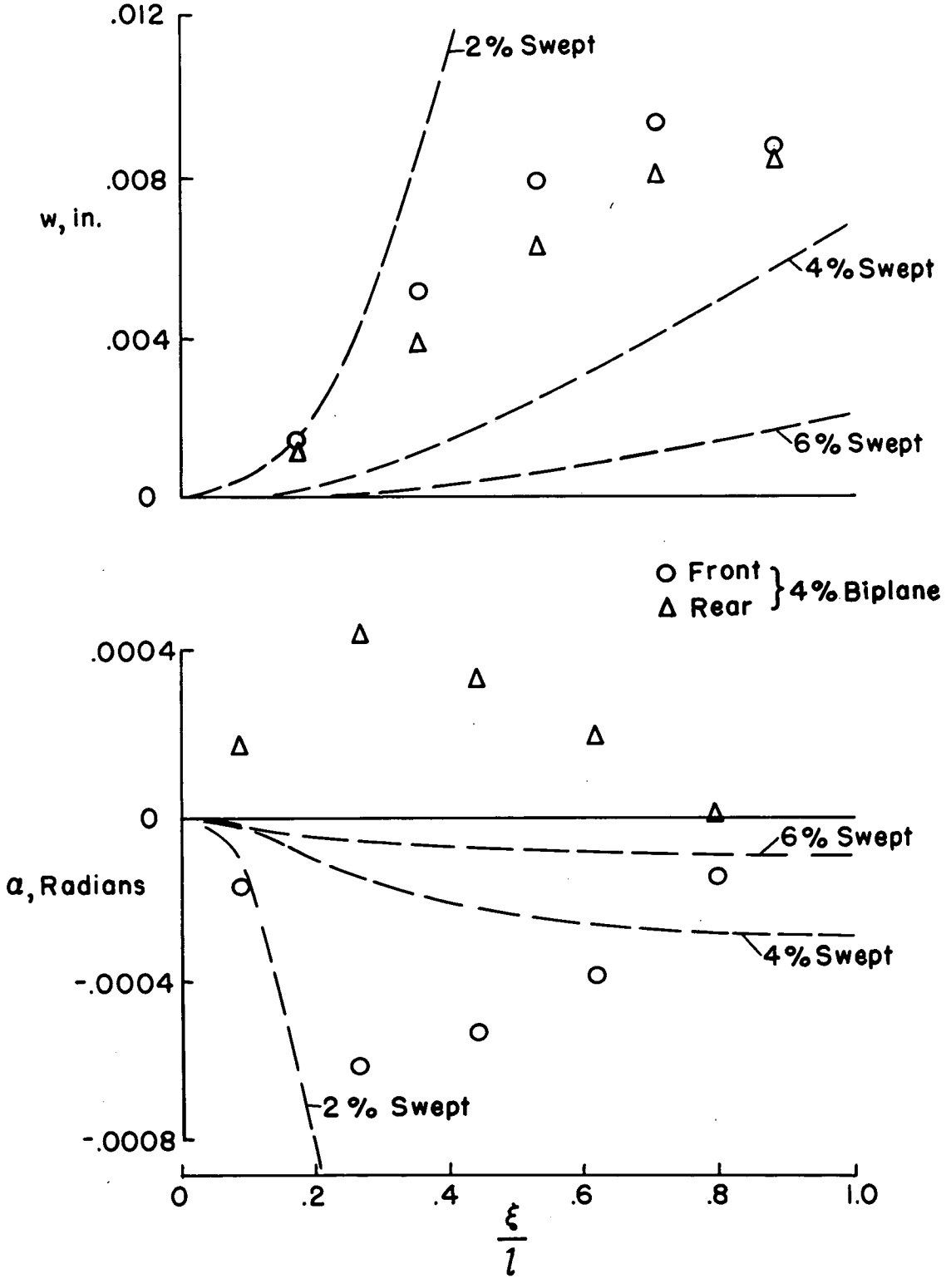

Figure 13.- Deflections and angles of attack of swept biplane wing and swept monoplane wings for 20.03-pound lift load elliptically distributed.

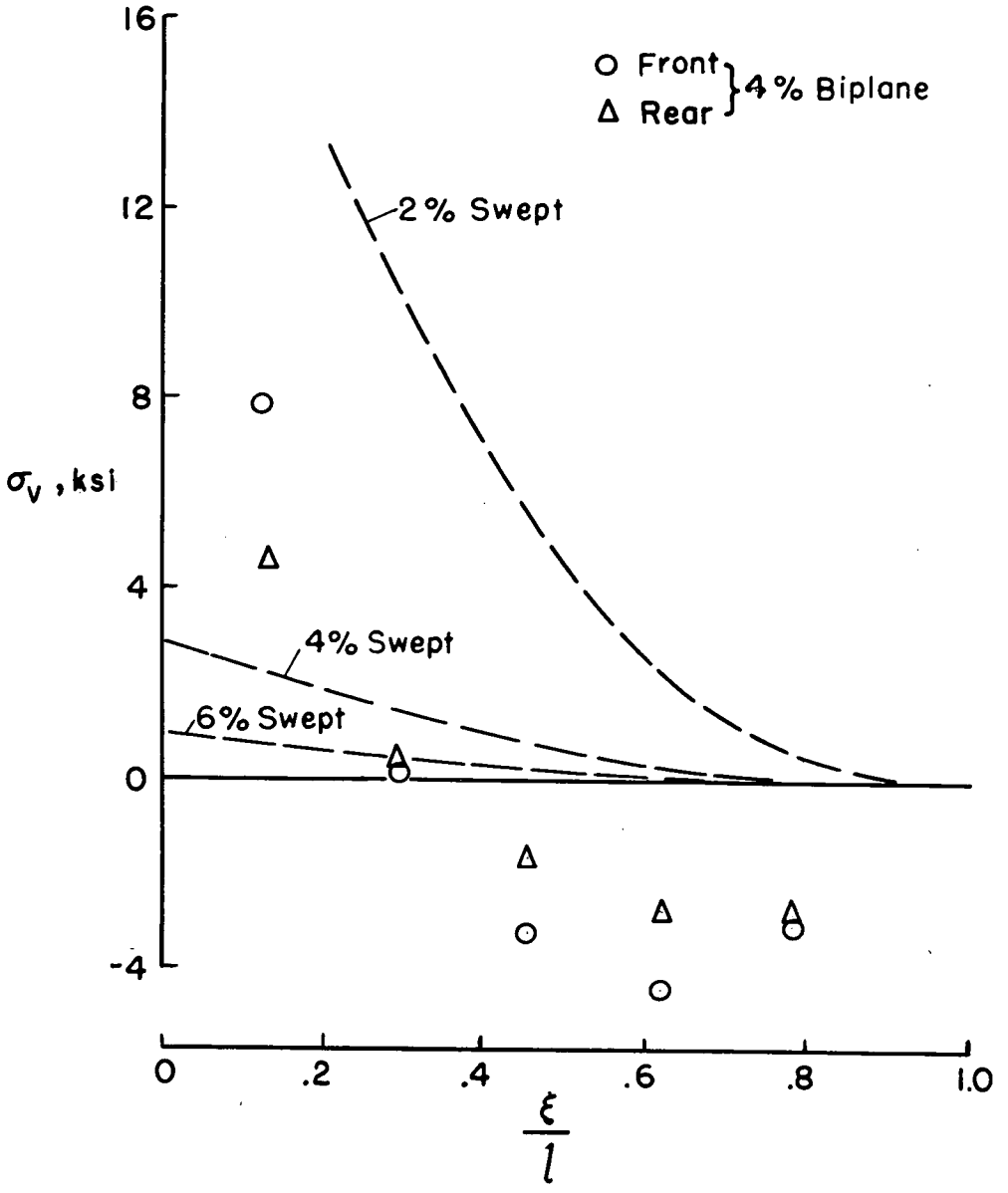

Figure 14.- Stresses of swept biplane wing and swept monoplane wings for 20.03-pound lift load elliptically distributed.

NACA-Langley - 8-3-54 - 350